ESO-906

Fermilab Library
0 1160 0023992 5

ESO-906

EUROPEAN SOUTHERN OBSERVATORY

SCIENTIFIC PREPRINT no.906

OBSERVATIONAL ASPECTS OF HERBIG-HARO JETS

Bo Reipurth and S. Heathcote

February 1993

OBSERVATIONAL ASPECTS OF HERBIG-HARO JETS

Bo Reipurth
European Southern Observatory
Casilla 19001
Santiago 19
Chile

Steve Heathcote
Cerro-Tololo Inter-American Observatory
Casilla 603
La Serena
Chile

Abstract. The highly collimated Herbig-Haro jets, which in some cases are found to emanate from very young stars, are reviewed in the light of observations at optical, infrared and radio wavelengths. Because these jets principally radiate with line-emission, a large number of observational techniques can be employed to give insight into the physical conditions in the flows. The case of the HH 34 complex, one of the finest such systems, is reviewed in detail. A more poorly collimated and presumably more evolved flow, HH 90/91, is discussed for comparison. The double jet in the HH 1/2 region is presented in terms of a binary central source with individual disks around each component. Recent VLA observations of thermal and non-thermal jets from embedded young stars are highlighted, and finally the nature of the driving sources is discussed.

1. Introduction

It is now ten years since the first Herbig-Haro jet, the spectacular jet in the HH 46/47 complex, was recognized as such by Dopita *et al.* (1982). This jet remains one of the finest known, and in the intervening years it has been studied in great detail (e.g. Graham & Elias 1983, Meaburn & Dyson 1987, Hartigan *et al.* 1990, Reipurth & Heathcote 1991). Located in a dense Bok globule in the Gum Nebula (Fig. 1), it displays a geometry which has now been recognized as archetypical: from a newborn star, still shrouded in placental material, emerges a supersonic well-collimated jet, which terminates in a bright working surface, at the point where it rams into the ambient medium. Further out along the flow axis one encounters a larger, more diffuse bow shock, dating from a previous cycle of activity of the energy source and now gradually fading. On the opposite side of the globule, one sees a counter jet and a counter bow shock, much fainter because of local extinction.

Invited review presented at the *Astrophysical Jets* symposium held at the Space Telescope Science Institute in Baltimore on 12–14 May 1992

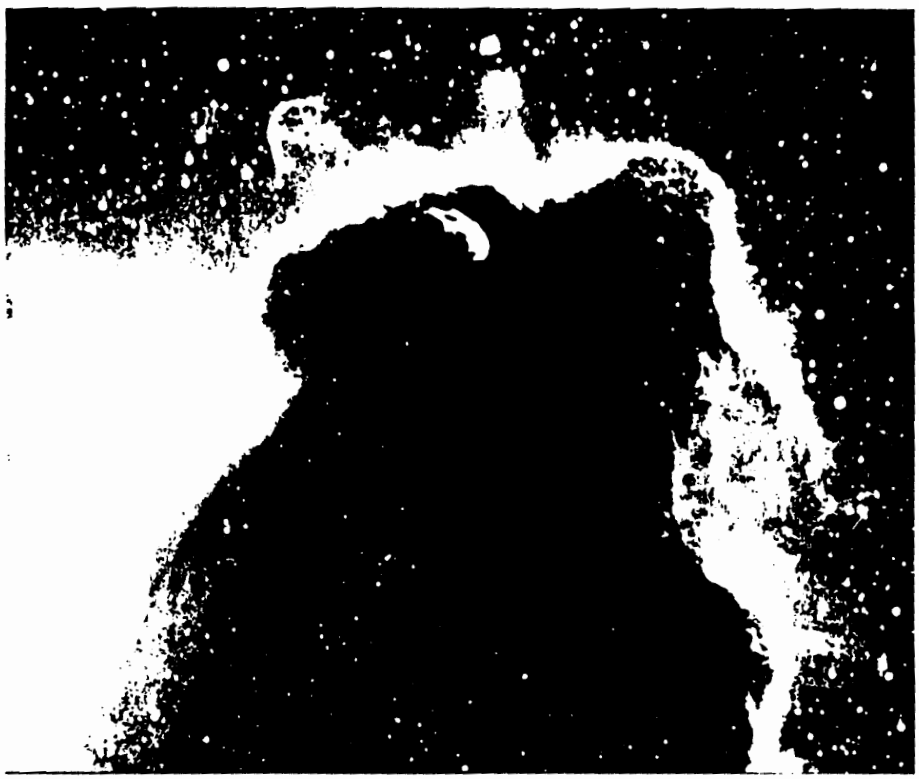

Figure 1. A CCD image taken through an Hα filter of the Bok globule that contains the young embedded star from which the HH 46/47 jet complex emanates. The Herbig-Haro system is partly blended with the bright rims of the globule, which are excited by UV radiation from luminous O stars at the centre of the Gum Nebula. From Olberg *et al.* (1992).

Far from all Herbig-Haro objects display this ideal morphology. Since their discovery more than forty years ago by Herbig (1950, 1951) and Haro (1952, 1953), close to 175 HH objects have been discovered, and new ones continue to be found (Reipurth 1993). Most of these shocked flows have twisted and tortured shapes, suggesting that their development is defined by complex flow patterns. A minor fraction, however, shows the highly collimated morphology of HH 46/47, and these very young Herbig-Haro jets are the center of focus of this review.

Jets from young stars offer investigators a number of advantages relative to their extragalactic cousins: first and foremost, their radiation is principally line-emission rather than a continuum, opening up a vast field of observational techniques which probe their physical conditions and the processes which govern them. Also they are nearby and generally bright, allowing detailed studies, and they evolve on relatively short timescales, permitting direct observations of evolutionary changes.

In the following, we present a detailed and critical discussion of one of the finest Herbig-Haro jets known, the HH 34 jet, illustrating by way of example what can be learned about Herbig-Haro jets with current observational techniques. We then discuss a case of what appears to be an evolved jet system. A unique case of a double jet emanating from a newborn binary system is then presented, followed by a discussion of radio observations of Herbig-Haro jets from low mass as well as high mass young stars.

Finally, we briefly discuss the sources which are responsible for jets in star forming regions.

2. The HH 34 Jet Complex

The HH 34 complex, located in the L1641 cloud in Orion, is one of the finest known examples of a highly collimated, bi-polar outflow delineated by HH objects. An overview of the entire HH 34 complex is provided by the two very deep, wide-field CCD images taken from the study of Reipurth & Heathcote (1992) which are reproduced in Fig. 2. Both images were obtained at the ESO 3.6-m telescope through two similar narrow-band interference filters; that used for Fig. 2a isolated the [SII]6717,31 doublet, while that used for Fig. 2b, transmitted Hα (plus the nearby [NII] lines). Although included amongst the earliest catalogued HH objects (Herbig 1974), HH 34 was only studied in detail following the discovery of an associated, highly collimated jet (Reipurth 1985a). The almost straight knotty jet, most prominently seen in the [SII] image, has a total length of 26″ which at an adopted distance of 460 pc corresponds to 0.06 pc in projection. It emanates from a faint heavily reddened emission line star and points exactly towards HH 34, the bright parabolic nebulosity near the center of the frame. This remarkable alignment, together with the arcuate morphology of HH 34 led Reipurth *et al.* (1986) to identify HH 34 as the working surface where the jet impinges on the ambient medium. The apex of the HH 34 bow shock lies $\sim$ 110″ (0.24 pc in projection) from the source.

At very nearly the same distance from the source in the opposite direction and precisely on the axis of the flow, is a fainter counter bow shock, HH 34-North, discovered by Bührke *et al.* (1988). The jet and HH 34 are both blue-shifted while HH 34-North is red-shifted. No red-shifted counterpart of the jet has yet been identified. Were this non-detection based solely on emission lines in the visible such as [SII]6717,31 this might simply be ascribed to higher extinction toward the receding lobe. However, no counter jet was detected in the [FeII]1.64 μm emission line, although the jet is a strong emitter in this transition (Stapelfeldt *et al.* 1991). A counter jet having an intrinsic brightness equal to that of the jet would have to be obscured by at least 3 mag at 1.64 μm, corresponding to $A_V \sim 17$ mag, to have escaped detection. While this is not excluded, one must at least consider the possibility that either the outflow itself, or conditions in the ambient medium, are different on the two sides of the source, so that the counter jet is intrinsically faint.

Two further bow shocks have been identified in the approaching lobe of the outflow (Reipurth & Heathcote 1992). One of these, knot O, is located mid-way between the source and HH 34, the other, HH 34X, is the very low surface brightness nebulosity a further 50″ along the axis of the flow beyond HH 34. Both these knots clearly possess an arcuate morphology very similar to that of HH 34 albeit on a smaller scale.

A comprehensive study of the kinematics of the HH 34 complex has recently been completed by Heathcote & Reipurth (1992). They present both radial velocities measured from high resolution long slit spectra and proper motions derived from CCD images collected over a period of more than eight years. An independent proper motion study, based on a shorter four year baseline, has been performed by Eislöffel and Mundt (1992). Figure 3 taken from Heathcote & Reipurth (1992) provides a convenient summary of the proper motion results. These observations provide the final conclusive proof that the HH 34 flow is indeed bi-polar and attest to the high degree of collimation inferred on morphological grounds. The jet, knot O and HH 34 (no measurement

Figure 2a A wide field image of the HH 34 complex obtained at the ESO 3.6m telescope through a [SII] filter. North is up and East to the left. The HH 34 jet emanates from the source which is visible as a faint star. The source is bracketed by two bow shaped nebulae, HH 34 the brighter one to its south, and HH 34-North near the upper right hand corner of the frame. Knot O the working surface of the jet lies midway between the source and HH 34, while HH 34X is the very faint knot further along the flow axis to the south.

Figure 2b The same region shown in Fig. 2a as seen through an Hα filter. Note that while the jet is much fainter in this image, HH 34 is much brighter and more extensive. In the bottom left hand corner of the frame is another, probably unrelated group of knots, HH 134. The long luminous tongue extending from the upper left corner is part of the "Orion streamers", a shock excited nebulosity. Two reflection nebulae located to the east and west of the source are illuminated by two other young stellar objects which have formed in the same cloud core as the HH 34 source, while the bright star further to the west is another young star V801 Ori. From Reipurth & Heathcote (1992).

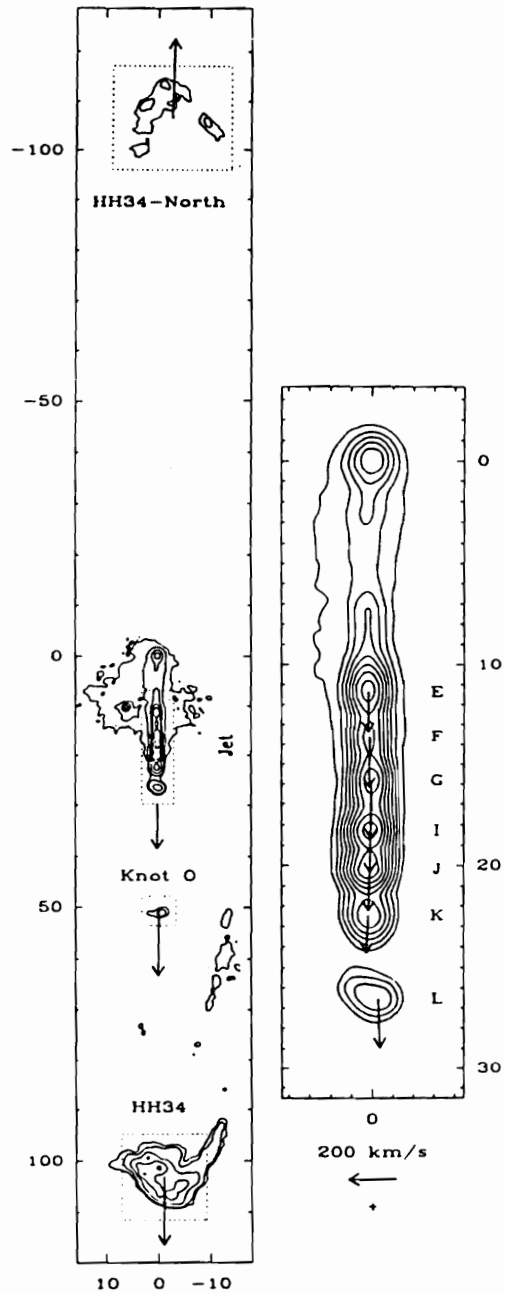

Figure 3. The proper motion vectors for various parts of the HH 34 complex are shown superposed on a contour diagram. The coordinate axes are labeled in arcseconds measured from the position of the exciting source; one arcsecond corresponds to a linear distance of 6.9×10^{15} cm or 2.23×10^{-3} pc for an assumed distance to HH 34 of 460 pc. The left hand panel covers the entire complex (except for HH 34X), the arrows indicating the motions over an interval of 100 years. The inset at right shows a 4× enlargement of the region around the jet; the superposed vectors give the motions of the individual knots over a period of 25 years. Note that the length of the arrow representing a given proper motion is the same in the two panels. The cross shows the 1σ positional uncertainty which results from the typical proper motion error of 0.7 $''$/100 yrs. The displacement corresponding to a transverse velocity of 200 km s^{-1} at the adopted distance is also shown. From Heathcote & Reipurth (1992).

could be made for HH 34X) each move southward away from the source *exactly* along the axis of the flow with transverse velocities of 190 km s^{-1}, 275 km s^{-1} and 285 km s^{-1}, respectively, while HH 34-North moves in the diametrically opposite direction at a transverse velocity of 350 km s^{-1}. For all these objects, the component of the proper motion orthogonal to the axis of the flow is smaller than the errors of measurement ($\sim \pm 20$ km s^{-1}) leading to an upper limit to any deviations of the motion from the axis of the flow of $\pm 10°$ (3σ).† As discussed further below, the measured tangential and radial velocities imply that the flow axis is inclined to the plane of the sky at an angle of about 30°.

In the remainder of this section we will discuss HH 34 and the jet in detail as prototypical examples of a working surface and of an HH jet, respectively. We will then discuss the evolution and energetics of the HH 34 outflow as a whole.

2.1 The HH 34 Working Surface

HH 34 is believed to correspond to the "working surface" where the supersonic jet collides with slower moving ambient gas (Reipurth *et al.* 1986). It should then consist of two shocks — the bow shock which accelerates the ambient medium and the Mach disk which decelerates the jet. If the jet is denser than the ambient medium then the bow shock will be the stronger of the two shocks and will hence be brighter and will have a higher excitation spectrum than the Mach disk, while the converse is the case for a light jet. Nonetheless, for parameters believed to be appropriate for HH jets, the bow shock and Mach disk should both be visible over a very wide range of density ratios (Hartigan 1989). Reipurth & Heathcote (1992) have shown that, in the case of HH 34, one can use the difference in excitation to separate and identify the two shocks. Fig. 4, taken from this study, shows the result of subtracting a [SII] and an Hα image from one another. Regions in which [SII] is brighter than Hα, as expected for a weak shock, appear white, while Hα bright regions are black. While most of HH 34 is Hα strong there is a small patch of [SII] strong emission *precisely* on the axis of the jet. This region of low excitation emission also has much lower electron density than its surroundings and is kinematically as well as spatially distinct (Heathcote & Reipurth 1992, Morse *et al.* 1992). There is thus little doubt that it does indeed correspond to the Mach disk, while the remainder of the emission comes from the bow shock. Since the Mach disk is the weaker of the two shocks the jet must be of greater density than the ambient gas. The Hα-[SII] difference technique has also been successfully used to locate the Mach disk in several bow shocks in the HH 46/47 and HH 111 complexes (Reipurth & Heathcote 1991, Reipurth *et al.* 1992).

Theoretical models of radiative bow shocks have been developed by a number of workers (e.g. Hartmann & Raymond 1984, Raga & Böhm 1985, Raga 1986, Hartigan *et al.* 1987). These models explain a number of features of HH 34 quite apart from its obvious arcuate morphology. A key characteristic of a bow shock is that the shock strength varies along the bow, being a maximum at the apex (where the shock is normal) and decreasing monotonically along the wings as the shock becomes increasingly oblique. Bührke *et al.* (1988) showed that [OIII] emission, which traces the gas of

† Eislöffel & Mundt (1992) report a substantial transverse motion of HH 34-North which is not seen in our data. Also, HH 34-North lies exactly on the tightly defined morphological axis, along which both HH 34 and the jet move, so it seems most unlikely that this sideways motion could be real.

Figure 4. An Hα - [SII] difference image of the HH 34 jet. Hα strong regions are black, and [SII] bright regions are white. The low excitation of the jet is readily apparent as is the division of HH 34 into two zones of different excitation which are believed to correspond to the bow shock (black) and Mach disk (white). Stars do not completely disappear in the subtraction because the filters have somewhat different band widths and hence pass slightly different amounts of continuum. From Reipurth & Heathcote (1992).

highest temperature and excitation, is indeed confined to a small region near the apex of HH 34. They also used long slit spectroscopy to coarsely sample the radial velocity field and electron density distribution and confirmed that the excitation, density and velocity do decline as expected along the western wing of the bow shock (the situation in the eastern wing is confused because of strong emission from the Mach disk). In an important recent study, Morse *et al.* (1992) have used an imaging Fabry-Perot interferometer to obtain fully sampled maps of the velocity field, electron density and excitation over the entire extent of HH 34 which they then compare to the predictions of a 3D bow shock model. Figure 5 taken from this study shows the comparison be-

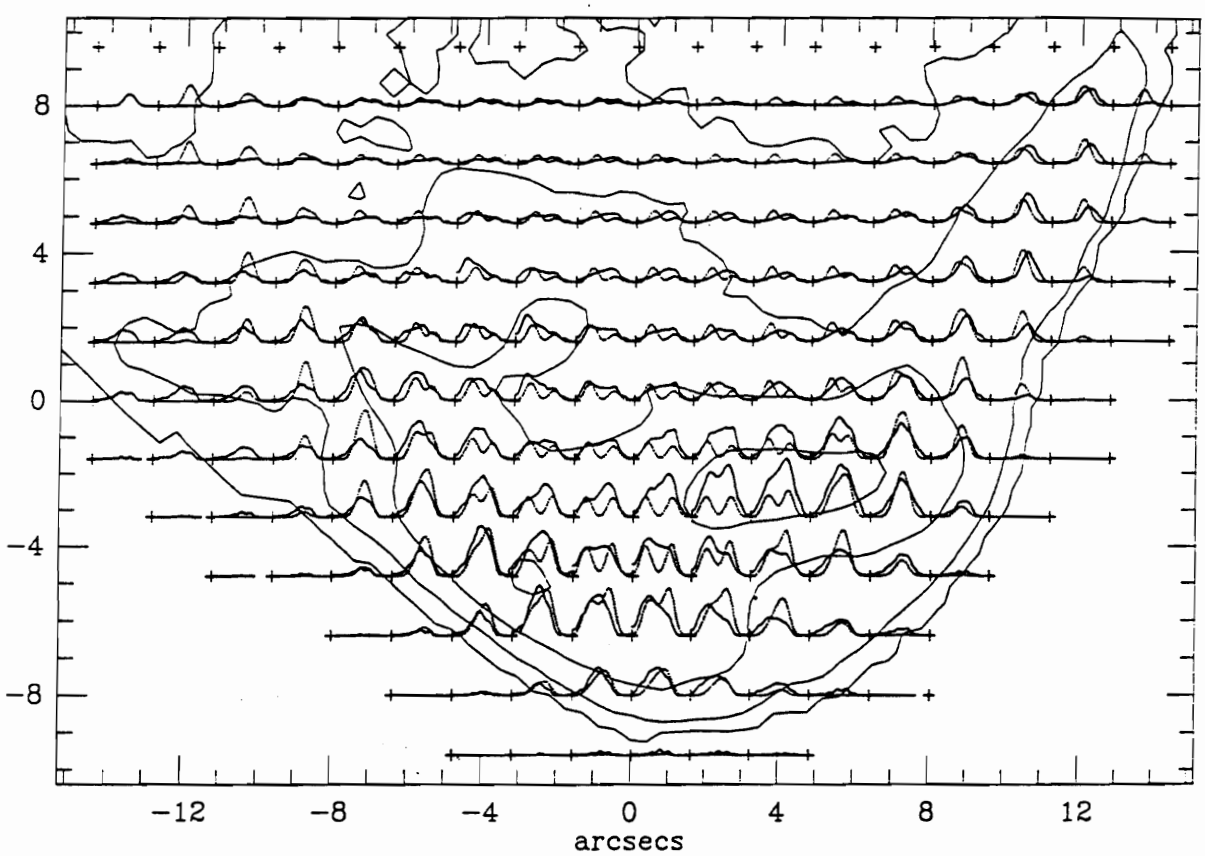

Figure 5. The velocity field within the HH 34 working surface derived from imaging Fabry-Perot observations obtained at the CTIO 4.0m telescope. The underlying contours show the Hα intensity integrated over all velocities. The solid curves show the observed Hα spectra at a grid of positions covering HH 34. Each spectrum runs from -200 km s^{-1} to $+80$ km s^{-1} heliocentric velocity, with blue wavelengths to the left. Note the multi-peaked profiles in the core of HH 34. The dotted curves are spectra derived from a bow shock model with a shock velocity of 160 km s^{-1} moving at an angle of 30° to the plane of the sky. A systematic blue-ward shift of 50 km s^{-1} has been applied to the model profiles in order to align them with the data. This offset indicates that the pre-shock medium ahead of HH 34 streams away from the source at a velocity of $\sim$150 km s^{-1}. From Morse *et al.* (1992).

tween the observed and predicted velocity fields for Hα. Morse *et al.* (1992) find that the bow shock model is generally quite successful in reproducing both qualitative and quantitative aspects of their comprehensive data set.

The shock velocity of the HH 34 bow shock has been estimated in a number of ways. Based on purely geometric considerations the full width at zero intensity of the lines

emitted by an ideal bow shock is approximately equal to the shock velocity (Hartigan *et al.* 1987). In this way one finds $V_{sh} \sim 160 - 200$ km s^{-1}depending on the emission line considered (Bührke *et al.* 1988, Heathcote & Reipurth 1992, Morse *et al.* 1992). By comparing various diagnostic line ratios with the predictions of shock models, Bührke *et al.* (1988) obtained $V_{sh} \sim 120 - 170$ km s^{-1}. As discussed by Morse *et al.* (1992), a strong constraint on the shock strength is provided by the distribution with position and velocity of [OIII]5007 emission because significant [OIII] emission is only produced when the normal component of the shock velocity exceeds ~ 100 km s^{-1}. They derive $V_{sh} \sim 125 - 140$ km s^{-1} from the observed extent of the [OIII] emission and argue that if the shock velocity were as high as 200 km s^{-1} [OIII] emission should be detected far back along the wings of the bow shock.

Morse *et al.* (1992) also discuss how other key parameters of the bow shock can be determined by comparing their observations to bow shock models. Given the shock velocity, the density of the ambient material entering the bow shock can be estimated from the observed Hα luminosity. Similarly the pre-shock magnetic field can be estimated by comparing the post-shock electron density derived from the observed [SII]6717,31 line ratio to the compression across the shock expected for different field strengths. In this way they estimate $n_0 \sim 65\ cm^{-3}$ and $B_0 \sim 10 - 20\ \mu G$. A magnetic field of this strength plays an important role in limiting the compression behind the shock and hence broadening the cooling zone. It is, however, far too weak to have any effect on the large scale dynamics of the HH 34 flow.

Not surprisingly, given the quite idealized nature of the bow shock models, there are also significant discrepancies. While the trailing wings of HH 34 are smooth and symmetric, near its tip HH 34 has a somewhat distorted outline. In particular the apparent apex is displaced laterally relative to the Mach disk. In addition HH 34, like many other HH objects, consists of several prominent condensations embedded in a more tenuous envelope while no such internal structure is predicted for an ideal bow shock. Fig. 5 also shows significant departures from the smooth velocity field predicted by the models. More realistic time dependent numerical simulations (Raga & Böhm 1987) show that thermal instabilities can create internal structure within radiatively cooling bow shocks. Similarly models of radiatively cooling jets show that dynamical instabilities are important in the working surface, which consequently should have a complex time-dependent structure (Blondin *et al.* 1990). The ambient medium may also be inhomogeneous leading to further departures from the ideal model.

Heathcote & Reipurth (1992) have measured the proper motion of HH 34 as a whole using a cross-correlation technique and derived a tangential velocity of 285 km s^{-1} for an assumed distance of 460pc. This motion is directed *exactly* along the axis of the flow (as defined by a line joining the source to the Mach disk) the cross motion being smaller than the formal measurement error of ± 10 km s^{-1}. Eislöffel & Mundt (1992) measured motions for the individual knots in HH 34. The vector mean of their tangential velocities is 265 km s^{-1} (after correcting to the same assumed distance) and is again directed along the flow axis to within the measurement errors. The dispersion of the knot velocities around the mean is ~ 100 km s^{-1} in each direction, rather greater than the typical uncertainty ~ 40 km s^{-1} of the individual values. The excellent agreement between these two independent studies is most encouraging.

In principle one can combine the measured transverse and radial velocities for the HH 34 bow shock in order to calculate the space velocity of the bow shock, V_{BS} and the angle its motion makes to the plane of the sky, θ. However, if the condensation structure results from dynamical and thermal instabilities it is difficult to know how

the motion of any individual knot relates to that of the working surface as a whole. As argued by Heathcote & Reipurth (1992) the Mach disk is singled out because it must lie on, and should move along, the true axis of the system. In addition, its low excitation spectrum assures us that the Mach disk is a very weak shock and thus can only cause small perturbations in the flow. They therefore used the transverse motion of HH 34 as a whole, together with the radial velocity they measured for the Mach disk emission to obtain $V_{BS} \sim 330$ km s^{-1} and $\theta \sim 31°$; essentially identical results $V_{BS} \sim 370$ km s^{-1} and $\theta \sim 28°$ are obtained if the tangential velocities derived by Eislöffel & Mundt for the individual knots comprising the Mach disk are used instead. For an ideal bow shock, the radial and transverse velocity of the apex should also yield the true space motion. Eislöffel & Mundt, therefore, used the motion of Knot B, the condensation closest to the apex of HH 34, to obtain $V_{BS} \sim 400$ km s^{-1} and $\theta \sim 23°$. However, as already noted, the apparent apex of HH 34 is displaced laterally with respect to the axis of the flow and the radial velocity field in this region is quite poorly reproduced by bow shock models (see Fig. 5) so that it is not at all clear that the motion of knot B reflects that of the bow shock. In summary, it appears that HH 34 moves at a space velocity of about 330 km s^{-1} at an angle of approximately 30° to the plane of the sky. These quantities can, however, only be determined to an accuracy of ± 50 km s^{-1} and $\pm 10°$ because of the *intrinsic* velocity dispersion within HH 34 and concomitant questions of interpretation.

If HH 34 moved into a stationary medium then the shock velocity, V_{sh} should be equal to its space velocity V_{BS}. Instead we see that V_{BS} is much greater than even the largest estimate of V_{sh} given above and is in serious conflict with the [OIII] constraint. As discussed by Heathcote & Reipurth (1992) this discrepancy can be explained if rather than being stationary, the gas ahead of HH 34 streams away from the source. Consistent with this suggestion they detected very faint emission in the region just ahead of the apex of HH 34 and suggested that this might come from pre-shock gas photoionised by the UV radiation leaking from the bow shock. If this pre-shock gas flows along the axis of the HH 34 system, then its observed radial velocity, -85 km s^{-1}, corresponds to a velocity of recession from the source of $V_0 \sim 170$ km s^{-1}. The shock velocity would then be $V_{sh} = V_{BS} - V_0 \sim 160$ km s^{-1} in good agreement with the values quoted above. Eislöffel & Mundt (1992) drew attention to a faint knot ahead and to one side of the apex of HH 34 with a tangential velocity of ~ 73 km s^{-1} which might also form part of this pre-shock flow.

Motion of the pre-shock medium also explains another long standing discrepancy between bow shock models and the observations of HH 34. Bührke *et al.* (1988) noted that in HH 34 the line profiles are shifted systematically blueward compared to what would be expected for a bow shock moving at an angle 30° to the plane of the sky. This was confirmed by Morse *et al.* (1992) who were also forced to suppose that HH 34 advances into a moving medium in order to bring their bow shock model into agreement with the observed velocity field. They found the best overall match for a bow shock velocity $V_{sh} \sim 140$ km s^{-1} and an ambient medium velocity $V_0 \sim 150$ km s^{-1} in excellent agreement with the values derived by Heathcote & Reipurth (1992).

The postulated streaming of the pre-shock gas is entirely natural when one considers that HH 34 follows in the wake of an older bow shock HH 34X (Reipurth & Heathcote 1992). An analogous situation has been found in the case of HH 46/47 (Hartigan *et al.* 1990, Reipurth & Heathcote 1991, see also Raga *et al.* 1990) and HH 111 (Morse *et al.* 1993), and might also explain the discrepancy between the proper motion and shock velocity of HH 1 (Raga *et al.* 1988).

2.2 The HH 34 Jet

Fig. 6 provides a close up view of the HH 34 jet based on a sum of very deep [SII] images obtained in good seeing. Although shock excited emission can be traced all the way back to the source, for the first 10″ the jet is quite faint. Beyond this is a much brighter section about 15″ long containing eight almost stellar knots (E to L). The jet then fades abruptly and a gap containing only extremely faint diffuse knots separates the tip of the jet from the bow-shaped knot O some 50″ from the source. In principle these intensity variations could be due to changes in the amount of foreground extinction. However, the intensity of the [FeII] 1.64 μm line varies with distance from the source in the same way as does that of the [SII]6717,31 lines, despite the very large difference in the total extinction between these two wavelengths, implying that the observed brightness variation must be predominantly intrinsic in origin (Stapelfeldt *et al.* 1991).

The separation of the knots in the jet ranges between 1.2″ and 2.5″ with no obvious periodicity. Their sizes have been measured using various different deconvolution methods (Raga & Mateo 1988, Bührke *et al.* 1988, Raga *et al.* 1991). They have essentially constant widths (transverse to the axis of the jet) of around 0.6″ all the way from the source out to knot I, but beyond this the jet flares out so that its width has doubled by L. Close to the source the knots are somewhat elongated along the axis of the jet becoming more nearly circular with increasing distance. The spatial structure of Knot L is well resolved in Fig. 6 and it can be seen to have a distinct bow shape.

The jet is not perfectly straight. Where it emerges from the source, the axis of the jet differs by 5° from the mean axis of the flow defined by the bright knots, while even in the bright section of the jet some slight wiggling about this mean axis is evident. This wiggling becomes even more pronounced beyond knot L where one sees that the very faint knots M and N_1 to N_4 are displaced alternately to one side and then the other of the flow axis by an amount which increases steadily with distance.

The HH 34 jet, in common with most other known HH jets, has a characteristically low excitation spectrum with [SII]6717,31 very much stronger than Hα (Reipurth *et al.* 1986, Cohen & Jones 1987, Bührke *et al.* 1988). Such a spectrum implies that the shocks in the jet are extremely weak $V_{sh} \sim 15 - 30$ km s^{-1}. Fig. 7 shows the very deep high resolution echelle spectrum of the jet and of HH 34 obtained by Heathcote & Reipurth (1992). The radial velocity field in the jet is quite complex. As first noted by Bührke *et al.* (1988) two distinct velocity components are present in the bright section of the jet. Between the source and knot L, the fastest moving gas has a roughly constant radial velocity of ~ -100 km s^{-1}, however superimposed on this is a slow, crudely sinusoidal, modulation with a peak-to-peak amplitude ~ 17 km s^{-1}. Beyond knot L the velocity increases rather abruptly, reaching -133 km s^{-1} by knot O. The velocity of the second slower moving component increases smoothly from ~ -40 km s^{-1} near the source reaching nearly the same velocity as the faster moving material by knot G. Nonetheless the line profiles have asymmetric shoulders indicative of this two component structure out to knot L. The velocity dispersion in the "fast component" is ~ 16 km s^{-1} while that in the "slow component" is ~ 40 km s^{-1}. The two components also have different electron densities as derived from the [SII]6717/31 line ratio. The electron density of the fast component varies considerably with distance: it first falls precipitously from 3500 cm^{-3} in knot A to 740 cm^{-3} at D; it then rises slightly to a maximum of 1600 cm^{-3} at I, before falling once more to 80 cm^{-3} at M. That of the slow component is lower and more nearly constant at 500 cm^{-3} out to knot I, beyond

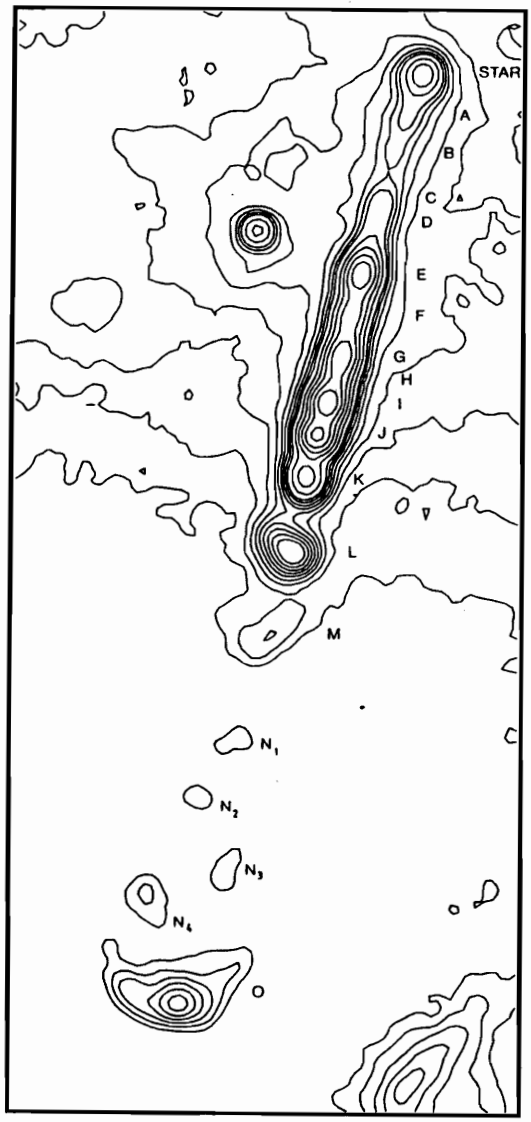

Figure 6. A contour plot showing details of the HH 34 jet based on a sum of [SII] images. The knots are identified. The strong gradient in the background is mostly due to the cone shaped reflection nebula which surrounds the source. From Reipurth & Heathcote (1992).

which its value falls in parallel with that of the fast component. This two component structure has been attributed to the entrainment of ambient material by the jet (Solf 1987, Bührke *et al.* 1988).

The proper motion vectors of the individual knots in the bright section of the jet as derived by Heathcote & Reipurth (1992) are shown in Fig. 3b. The transverse velocities of the knots range from 160 km s^{-1} to 250 km s^{-1} with a mean of 190 km s^{-1} (typical errors are $\pm$20 km s^{-1}) and are parallel to the axis of the jet to a truly remarkable degree. Generally consistent results were obtained by Eislöffel & Mundt (1992) although their values show somewhat more scatter due to a shorter temporal baseline.

If the knots in the HH 34 jet were parcels of gas moving ballistically, then the observed radial and transverse velocities would simply be the vector components of this motion parallel and perpendicular to the line of sight, respectively. In this "ballistic

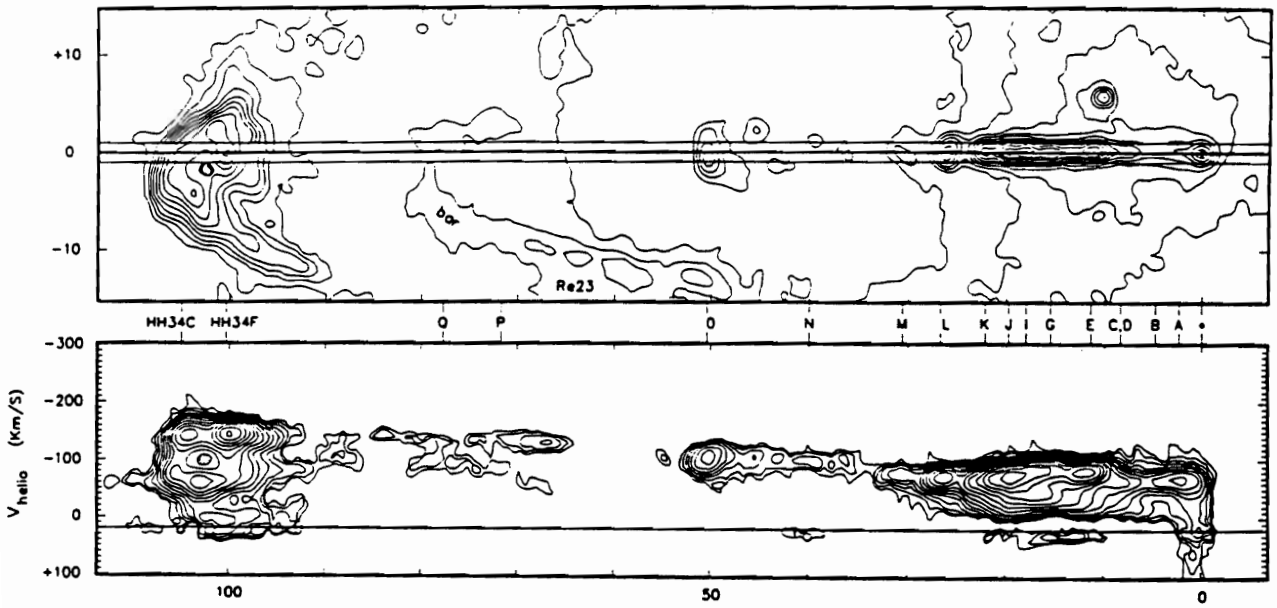

Figure 7. (a) A high resolution long slit echelle spectrum of HH 34 and its associated jet obtained with the CTIO 4.0m telescope. In order to improve the signal to noise ratio both members of the [SII]6717,31 doublet have been co-added to produce this diagram. The abscissa gives position along the spectrograph slit labeled in seconds of arc from the position of the exciting source. The ordinate is heliocentric radial velocity. Contours are logarithmic at intervals corresponding to a factor of $2^{1/2}$ in linear flux. The horizontal line at V_{helio}=20.5 km s^{-1} marks the velocity of the unresolved (FWHM$\sim$20 km s^{-1}) emission line due to foreground nebulosity. This has been carefully subtracted in order to render faint low velocity features in the HH object spectrum more easily visible. The molecular cloud in which HH 34 is embedded has V_{helio}=26.91 km s^{-1}. (b) An accurately scaled and aligned section from a nearly contemporaneous direct [SII] image of the same region. Again the contours are logarithmic at intervals of $2^{1/2}$ in linear flux. The solid line marks the center line of the spectrograph slit which was $2''$ wide. The principal emission features crossed by the slit are labeled. From Heathcote & Reipurth 1992).

limit" the data of Heathcote & Reipurth (1992) lead to a mean space velocity of $V_j \sim$ 220 km s^{-1} at an angle of $\theta_j \sim 28°$ to the plane of the sky for the knots in the bright section of the jet. Very similar values are obtained using the data of Eislöffel & Mundt (1992).

However, it is generally accepted that, instead, the knots represent radiative shocks excited within the jet. The very low excitation spectrum of the jet requires that these shocks are weak and hence only cause small perturbations in the velocity of the jet fluid, V_j. Thus radial velocity measurements will faithfully record the component of the jet's motion along the line of sight. Conversely, proper motion measurements refer to the propagation velocity of the shocks, V_p. If the internal shocks are normal, then their weakness requires that they travel along the jet at very nearly the fluid velocity. However, if they are oblique they could travel at a much slower velocity, or even be stationary, without violating this constraint. Thus one must consider these results in the light of dynamical models for the internal shocks.

Three models have been proposed to excite the pattern of more or less regularly spaced internal shock waves required to explain the appearance of the HH 34 jet and similar objects:

(1) A series of oblique "crossing shocks" results as a jet attempts to reach pressure equilibrium with its surroundings (Falle *et al.* 1987, Cantó *et al.* 1989, Raga *et al.* 1990); this could occur near the source if the jet is initially over-pressured, or where the pressure of the ambient medium falls abruptly e.g. at the edge of a cloud.

(2) Kelvin-Helmholtz instabilities at the boundary between the jet and its environment may excite a similar pattern of oblique shocks (Norman *et al.* 1984, Payne & Cohn 1985, Ray *et al.* 1988, Blondin *et al.* 1990).

(3) Supersonic perturbations in the outflow velocity from the source will create two-shock "internal working surfaces" which propagate along the jet (Raga *et al.* 1990, Kofman & Raga 1992, Raga & Kofman 1992, Norman 1993, Stone & Norman 1993).

The first of these mechanisms necessarily produces stationary shocks; the fact that proper motions are detected at all, then excludes it as a possibility in the case of HH 34. The second mechanism can produce knots which travel along the jet at a velocity substantially less than the fluid velocity. However, the numerical simulations of Norman *et al.* (1984) show that V_p/V_j increases with both increasing Mach number and with increasing jet-to-environment density ratio approaching unity in the limit of a highly supersonic heavy jet like the HH 34 jet. In addition for this model, the knot length-to-width ratios measured by Raga *et al.* (1991) can be used to estimate the obliqueness of the bi-conical crossing shocks. Based on such a calculation Heathcote & Reipurth (1992) find that V_p can differ from V_j by no more than ~ 60 km s^{-1} in order to have $V_{sh} \leq 30$ km s^{-1}. The third mechanism produces normal internal shock waves and hence the knots must travel at very nearly the fluid velocity if the shocks are to be as weak as observed. Thus in either of the latter two models the ballistic calculation should provide a good first estimate of the fluid velocity and orientation of the jet.

In their analysis, Eislöffel & Mundt (1992) take this discussion one step further and attempt to distinguish between the competing theoretical models. If the true angle the jet makes to the plane of the sky were known, then the quantity $V_p/V_j = V_t/V_r \tan\theta$ could be calculated directly from the observed tangential and radial velocities of the knots. They choose the value of θ on the, entirely reasonable, supposition that the jet and HH 34 move in the same direction. Adopting $\theta = 23°$ derived from the motion of the *apex* of HH 34 they find that $V_p/V_j \sim 0.5 - 0.7$ for the knots in the bright section of the jet; such low values are inconsistent with the internal working surface model,

but could be produced by K-H instabilities. However, if instead one takes $\theta = 31°$ as implied by the motion of the *Mach disk* then the same data leads to $V_p/V_j \sim 0.7 - 1.0$ values consistent with either model. One is forced to conclude that the uncertainty in the true direction of motion of HH 34, which as discussed in Sect. 2.1 is largely intrinsic rather than observational in nature, vitiates any attempt to distinguish between the two models in this way.

As described above the high resolution spectrum of the jet (Fig. 7) shows a general tendency for the radial velocity of the jet to increase with distance from the source, and on this is additionally superposed a roughly sinusoidal variation with a peak-to-peak amplitude of $\sim$ 17 km s^{-1}. These changes in the radial velocity are substantially greater than the errors of measurement and, given the straightness of the jet as seen in projection, are very unlikely to result from bending of the jet. Rather, it seems likely that the velocity of the jet does indeed vary by $\sim$ 20% along its length. For such a highly supersonic flow the most plausible origin for this trend would be a temporal variation in the outflow velocity from the source. The spatial scale of the velocity changes, $\sim 20''$ combined with the mean proper motion of the jet leads to a time-scale for the variation of the source of $\sim$200 years. If the knots in the jet do represent internal working surfaces, then the typical knot separation $\sim 2 - 4''$ implies that the outflow velocity from the source must also fluctuate on time-scales as short as $\sim 20 - 40$ years.

In the course of their proper motion study, Heathcote & Reipurth (1992) made the surprising discovery that knot J, near the tip of the jet, faded with time relative to the other knots. In their earliest epoch data, J was the brightest knot in the jet, while only eight years later it was much fainter than its neighbor I. Figure 8 shows the intensity ratio J/I as a function of time and, for comparison, the ratio G/I which is constant to within the errors. As described above it is precisely at the position of knot J that the brightness of the jet begins to decrease with increasing distance from the source and that the jet flares out. The electron density in the jet also starts to fall precipitously at this point while its radial velocity begins to increase. The observed *temporal* change in the brightness of knot J casts these *spatial* trends in a new light. At the measured rate of decline, knot J will have a brightness comparable to the current brightness of K in another $\sim$ 20 years. During this interval it will move $\sim 2''$ and will then be located very close to the present position of K. It is thus attractive to suppose that the knots are intrinsically similar in their properties, but that these evolve as the knots propagate along the jet. If this contention is correct then the density and width of knots near the tip of the jet should change by a measurable amount over an interval of only $\sim$ 10 years. It also implies that one can reconstruct the temporal evolution of an individual knot by measuring the spatial changes in the knot properties at any instant.

Why should the properties of the knots evolve as they propagate along the jet? Simple analytic calculations (Raga *et al.* 1990, Raga & Kofman 1992, Hartigan & Raymond 1993) suggest that such behavior may arise naturally in the internal working surface model. Indeed the beautiful simulations of time dependent jets presented by Norman in these proceedings (see also Stone & Norman 1993) bear an uncanny resemblance to what we observe in the case of HH 34. These computations show in detail the way in which initially subsonic perturbations in the input velocity of the jet grow into internal working surfaces which propagate ballistically along the jet for some distance before beginning to expand laterally and fade, gradually taking on the appearance of miniature bow shocks. Conversely, the observed trends might also be explained if near its tip the jet passes from a region of high ambient density into one of much lower density and pressure, as first considered by Reipurth *et al.* (1986). Near

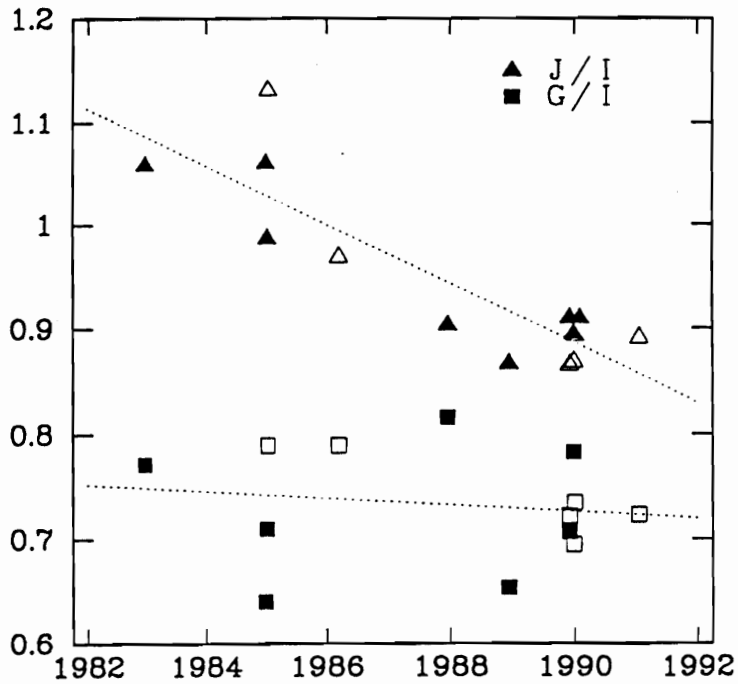

Figure 8. This figure illustrates the photometric variability of Knot J relative to other knots in the HH 34 jet. The brightness ratios J/I (triangles) and G/I (squares) are plotted as a function of time. Open symbols mark exposures obtained through a narrow-band [SII] filter, while solid symbols are for exposures through a broad-band Gunn-r filter which transmits [OI]6300,63 and Hα in addition to [SII]. From Heathcote & Reipurth (1992).

its base the jet might then be pressure confined, accounting for its constant width, but would begin to expand laterally near its tip as it adjusts to the lower pressure of its surroundings. Since the properties of the K-H instability depend on the jet-to-environment density ratio it is at least plausible that the characteristics of the internal shock waves would change in response to the changing environment, however detailed models would be required to confirm this. Both because the velocity of the HH 34 jet is *observed* to be variable, and because the time dependent jet model successfully explains several properties of the knots in this jet, we feel this model is to be prefered over the K-H instability model.

Reipurth & Heathcote (1992) suggested that knot O is the terminal working surface of the jet based on its obvious arcuate morphology (see Fig. 6). It also differs from the other knots in the jet by having a much larger velocity dispersion $\sim$ 80 km s^{-1} (Heathcote & Reipurth 1992). The Fabry-Perot data of Morse *et al.* (1992) show that the velocity field within Knot O changes from apex to wings as expected for a bow shock. The radial and tangential velocities measured for this knot imply that it moves at a space velocity of $\sim$ 300 km s^{-1} with an inclination of $\sim$ 26° to the plane of the sky. As with HH 34 one must suppose that the gas ahead of knot O streams away from the source in order to reconcile this large space velocity with the low shock velocity implied by its modest velocity dispersion and low excitation spectrum. This is not surprising given that knot O follows in the wake of HH 34.

2.3 Multiple Ejections in the HH 34 System

As discussed by Reipurth & Heathcote (1992), the presence of multiple bow shocks in the approaching lobe of the HH 34 bi-polar flow implies that the source has erupted episodically, each outburst giving rise to a new outflow. In order of increasing distance from the source these flows consist of the jet (for which Knot O is the working surface), HH 34 and HH 34X. The ages of the outbursts can be estimated by dividing the angular distance separating the working surface from the source by its proper motion. In this way one finds that the eruptions that created Knot O, HH 34 and HH 34X (assumed to have the same proper motion as HH 34) occurred 400 ± 30, 800 ± 15 and 1170 ± 30 years ago respectively; the dynamical age of HH 34-North, 710 ± 50 years is consistent given the errors with its being coeval with HH 34. Hence the interval between successive outbursts is $\sim$400 years. The decrease in the radial velocity of the jet with decreasing distance from the source suggests that the strength of the outflow has declined over the past 200 years. The smaller space velocity of knot O compared to that of HH 34 further suggests that this most recent event was less energetic than the one which preceded it.

Such recurrent activity of the source might be driven by accretion events similar to those supposed to be responsible for massive FUor outbursts as well as the more frequent but less powerful EXor events (Reipurth 1989b). The interval between FU Orionis eruptions is poorly known; the highly uncertain value of 10^4 years tentatively offered by Herbig (1977) applies to visible stars, and it is possible that such events are more common in earlier evolutionary stages (Reipurth 1990), or occur in series during periods of more active accretion. The total duration of the optical outflow phase in the life of young stellar objects has been estimated to be $\sim 2 \times 10^4$ years on statistical grounds (Mundt *et al.* 1987). During this time there could be several tens of such eruptions. The currently observable HH objects then result from the most recent few outbursts, those from earlier episodes having long since faded into invisibility.

Evidence for recurrent outbursts has been found in several HH complexes in addition to HH 34. Amongst the best documented cases are HH 111 (Reipurth 1989a, Reipurth *et al.* 1992, Morse *et al.* 1993), and HH 46/47 (Hartigan *et al.* 1990, Reipurth & Heathcote 1991) both of which contain multiple bow shocks. Interestingly, in both these systems it is found that the bow shocks driven by the more recent eruptions advance into a moving medium, exactly as does HH 34. As first proposed in the case of HH 46/47 (Hartigan *et al.* 1990, Reipurth & Heathcote 1991), it is most natural to suppose that this streaming motion has arisen as a result of the passage of earlier outflows. Each successive outflow will accelerate the material it overruns so that the gas in its wake, which represents the pre-shock gas for the next working surface, moves away from the source. In this way the velocity of the ambient medium could be built up to a substantial fraction of the flow speed through the cumulative effect of the many small impulses imparted by previous outbursts.

Heathcote & Reipurth (1992) have estimated the fluxes of mass, momentum and energy carried by the moving pre-shock medium ahead of HH 34 to be $\dot{M} \sim 1 \times 10^{-7}$ $M_\odot$ yr^{-1}, $\dot{P} \sim 1.7 \times 10^{-5}$ $M_\odot$ yr^{-1} km s^{-1} and $\dot{E} \sim 0.2$ $L_\odot$ respectively. There is considerable controversy about the values of these parameters for the HH 34 jet itself. This arises because in order to calculate the density of the undisturbed jet fluid from the observed electron density one must apply a large model dependent correction to account for partial ionization of the gas and for its compression by internal shock waves which together can lead to an uncertainty of as much as two orders of magnitude (c.f. Bührke *et al.* 1988 and Raga 1991). An independent estimate of the jet density has

been derived by considering the balance of the ram pressure across the HH 34 working surface (Morse *et al.* 1992), which appears to confirm the larger density favored by Raga (1991). If this larger density is correct then one obtains $\dot{M} \sim 3 \times 10^{-7}$ $M_\odot$ yr^{-1}, $\dot{P} \sim 5 \times 10^{-5}$ $M_\odot$ yr^{-1} km s^{-1} and $\dot{E} \sim 2$ $L_\odot$. This is then compatible with the idea that the ambient medium has indeed been set in motion by the passage of earlier outflows of similar strength to those presently seen. There would be considerable difficulty in understanding the acceleration of the ambient medium if instead the much smaller values suggested by Bührke *et al.* (1988) were correct.

Reipurth *et al.* (1986) did not detect a molecular flow associated with the HH 34 complex although this may be due to confusion by background emission in this very complex region. However, this HH flow is embedded in and we believe has, over its lifetime, accelerated a more extended neutral or ionized flow which carries a momentum flux falling within the range of values found for conventional molecular flows. This provides support for the idea (Raga and Cabrit 1993) that it is the very tenuous but highly supersonic HH flows driven by young stellar objects that entrain and accelerate gas in their surroundings and thus give rise to the much more massive but very slowly moving molecular flows (see also review by Stahler in these proceedings). An important determinant of the nature of the molecular outflow from a young stellar object may then be how close it lies to the surface of the parent molecular cloud. The jet from a deeply embedded source will interact with dense, molecular gas and will consequently drive a traditional molecular flow. Conversely in the low density environment at the edge of a cloud, the same jet might instead drive a less massive but much faster flow such as the one seen in the case of HH 34.

3. HH 90/91: An Evolved Jet System?

Only a small minority of HH flows show the perfect collimation of the HH 34 jet discussed in the preceding section. Mostly HH flows merely display a preferred direction, within which they exhibit a multitude of chaotic shapes of knots, wisps, bows and bullets, testifying to the complex flow patterns which excite them.

HH 90/91 is a case in point. Located at the edge of the L1630 cloud in Orion, the whole complex stretches over 580″, which at an assumed distance of 460 pc corresponds to 1.3 pc in projection, a very considerable size for an HH flow. Fig. 9 shows a mosaic of CCD images, each a sum of an Hα and a [SII] image, displaying the entire complex with its well defined flow axis, from a new study by Gredel *et al.* (1992). HH 90 is an outlying bow shock to the west. HH 91 is the complex object to the east. A faint near-infrared source has been found in the middle of HH 91. Proper motion measurements show that HH 91 is expanding towards east and west, away from the infrared source, with velocities of around 50 km s^{-1}. HH 90 is also moving away from this presumed driving source with about the same velocity. The eastern side of HH 91, which clearly has the morphology of a bow shock, has a dynamical age of about 2000 yr. At its present velocity HH 90 would have required about 24000 yr to reach the position it has today. Apparently the underlying source has had two separate phases of activity. Although HH 91 is symmetric about the central source, there is no visible counterpart to HH 90. However, the HH flow is located just west of the sharp boundary of the L1630 cloud, and it is very probable that an eastern counterpart to HH 90 could be

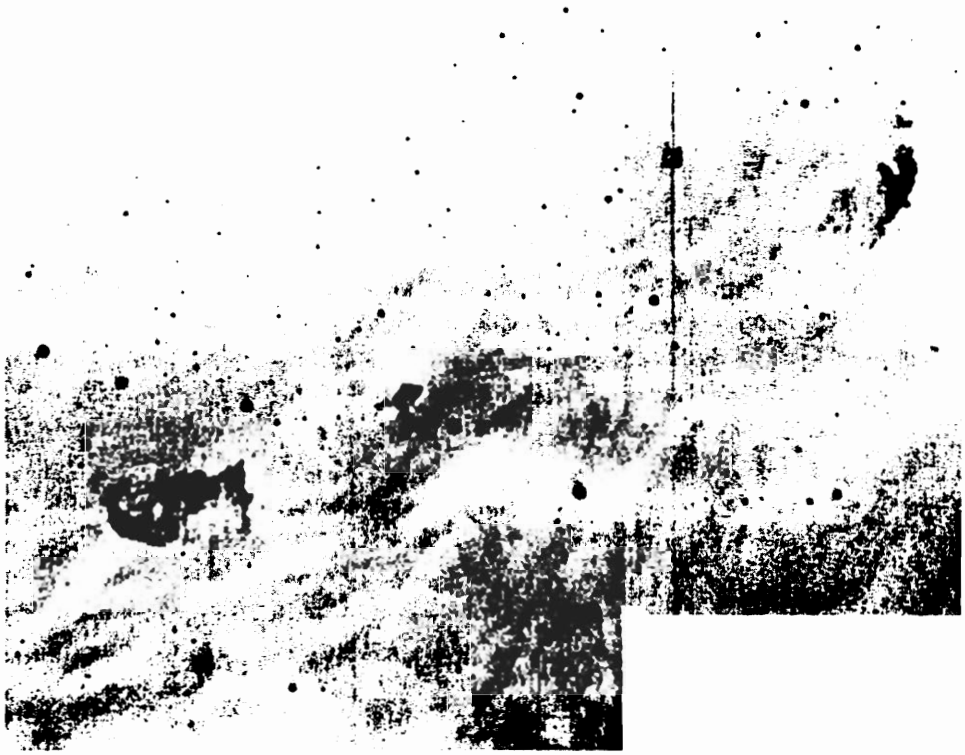

Figure 9. The HH 90/91 complex as seen on a mosaic of CCD images, each a sum of an Hα and a [SII] image. HH 90 is the large bow shock to the west, and HH 91 the intricate structure to the left. North is up and east is to the left. From Gredel *et al.* (1992).

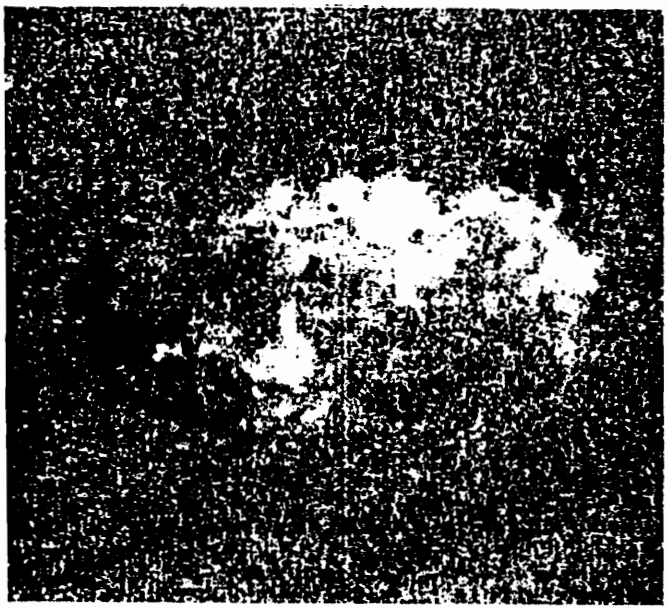

Figure 10. An Hα–[SII] difference image of HH 91. Hα–strong regions are black and [SII]–bright regions are white. The thin bow shock to the east has high excitation, as does the end point of the diffuse jet to the west. All the interior structures are weak, low-excitation shocks. North is up and east to the left. From Gredel *et al.* (1992).

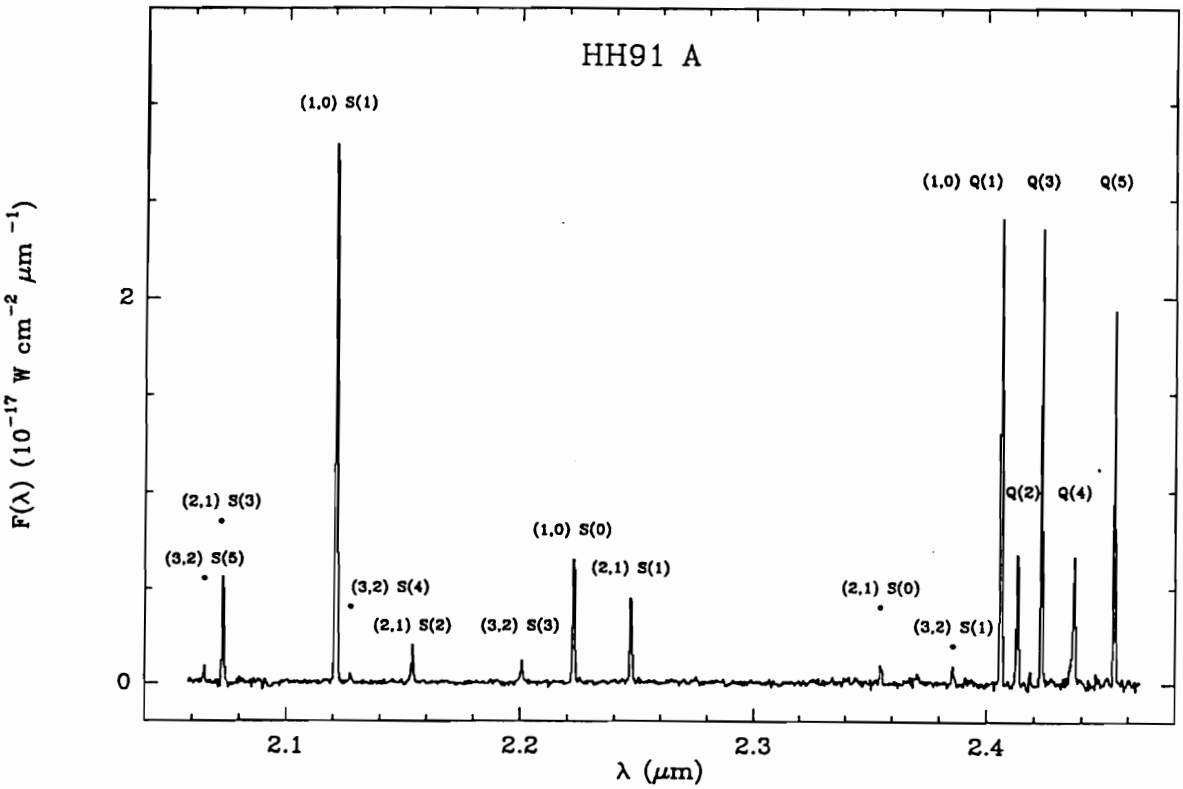

Figure 11. The 2−2.5 μm spectrum of HH 91A (the center of HH 91). A number of H_2 rotational lines arising in various vibrational bands are identified. Fluxes are in units of 10^{-17} W cm^{-2} μm^{-1}. From Gredel *et al.* (1992).

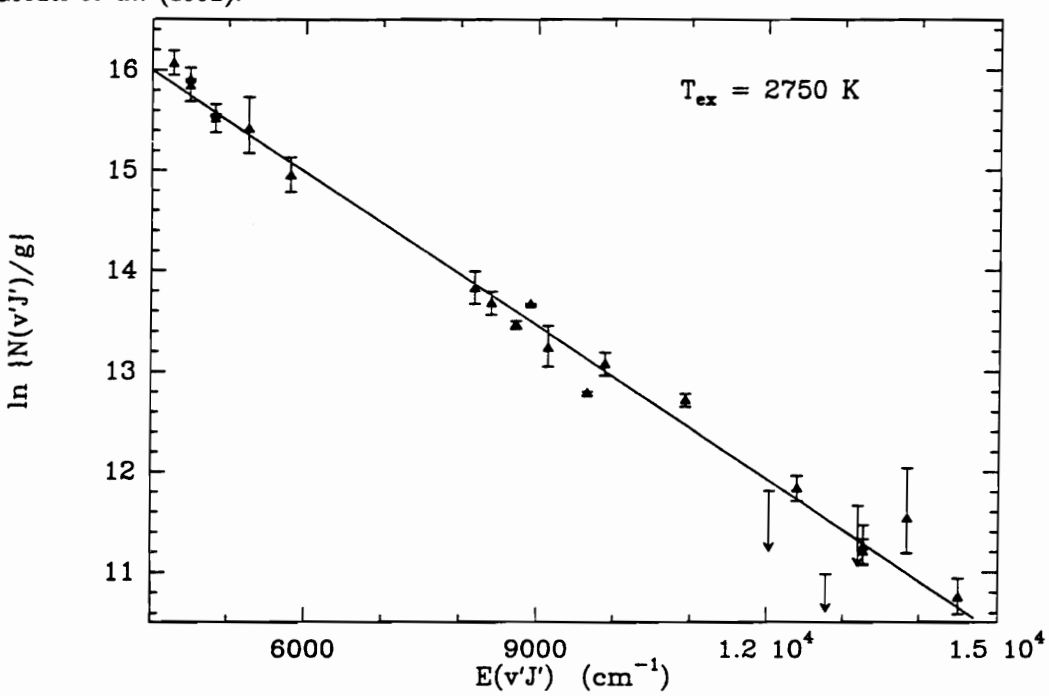

Figure 12. An H_2 excitation diagram for HH 91A based on the spectrum shown in Fig. 11. The straight line that fits the data well shows that the emission arises in a medium with a uniform excitation temperature of 2750 K. From Gredel *et al.* (1992).

hidden from view behind the cloud edge.

Figure 10 shows an Hα–[SII] difference image of HH 91, Hα-strong areas are black and [SII]-strong areas are white. To the west and, in particular, to the east the HH object is bordered by Hα-bright regions; in these places the flow impacts directly on the surrounding medium and the shocks are stronger. On the other hand, the whole central region predominantly emits in [SII], suggesting that these internal shocks are weak, presumably because the HH flow here follows in the wake of the eastern and western working surfaces.

In low-velocity weak shocks, infrared emission from molecular Hydrogen is often an important cooling mechanism. HH 91A, the central region of HH 91, is in fact the brightest HH object known in the rotational transitions that mainly arise in the S– and Q–branches of the (1,0) vibrational band at 2.2μm. Gredel *et al.* (1992) have made the first high resolution IR spectra that covers the wide wavelength range from 2 to 2.5μm (Figure 11). These H_2 measurements can be used to infer the temperature of the post shock region, if the vibrational and rotational population densities are all relaxed to a uniform excitation temperature T_{ex}. Figure 12 shows an H_2 excitation diagram for HH 91A, in which population densities $N(v'J')$ per statistical weight g are plotted versus the excitation energy $E(v'J')$ of the upper level of each transition; the slope of the points is proportional to T_{ex}^{-1}. The solid line is a fit to the data and represents a population distribution with $T_{ex} = 2750 \pm 300$ K. The excellent fit to a straight line shows unambiguously that molecular Hydrogen in HH 91A is thermalized to a uniform excitation temperature and that non-thermal processes like UV fluorescence are absent.

Because of the dusty medium from which HH flows emanate, extinction can be significant. The near infrared H_2 lines offer a tool to determine reddening of HH objects. If two emission lines arise from a common upper level, their intensity ratio is largely determined by the ratio of the transition probabilities and the line frequencies (for further discussion see Solf *et al.* 1988 and Gredel *et al.* 1992).

The flow in HH 91 is clearly rather poorly collimated. This may be related to the evolutionary state of the driving source, which was not detected by IRAS, nor in the 1300μm survey of Reipurth *et al.* (1993b). Also, no trace of CS emission around the source has been detected, although it is common that young stars with HH flows are still embedded in dense CS cores. It is thus conceivable that the HH 90/91 complex represents an HH flow in a fairly advanced state of evolution at a time when the source is about to loose its collimating powers, after which its wind will merely diffuse into space.

4. The Binary Jets in the HH 1/2 Region

The first two Herbig-Haro objects discovered were HH 1 and 2, found more than forty years ago by Herbig (1951) and Haro (1952). The region is seen in an Hα+[SII] CCD image in Fig. 13. Like HH 34, a variety of observations suggest that HH 1 is a bow shock in a highly collimated flow. HH 2 is the counter bow shock; its highly fragmented morphology may indicate that instabilities, perhaps thermal, are affecting this part of the flow (e.g. Raga *et al.* 1988). Accurate proper motions show that both objects move away from each other at highly supersonic velocities, of the order of 300 km s^{-1} and almost in the plane of the sky (Herbig & Jones 1981). The total dimension of this bipolar complex is close to 3 arcmin, which at a distance of 460 pc corresponds to almost 0.4 pc. Midway between the objects a deeply embedded source has been detected in the cm-wavelength range at the VLA (Pravdo *et al.* 1985). Two

Figure 13. The HH 1/2 region in Orion seen in a mosaic of CCD images, each a sum of an Hα and a [SII] exposure. HH 1 and 2 are two bow shocks moving in opposite directions from a central embedded source. A small jet emanates from this source towards HH 1. HH 144 is a long chain of faint knots moving to the west of the source region. North is up and east is left. From Reipurth *et al.* (1993a).

shock excited regions are found in the source region. One is a short jet, the HH 1 jet, which starts close to the source and points towards HH 1. The other consists of two small faint knots west of the source (Strom *et al.* 1985, Bohigas *et al.* 1985).

Figure 14 shows a contour plot from a [SII]6717/31 CCD image of the source region from a new study by Reipurth *et al.* (1993a). The HH 1 jet is short ($14''$, or 0.03 pc) and highly collimated, with a number of distinct knots, directed precisely along the axis defined by HH 1 and 2. There is a slight but unmistakable wiggling of the knots along the jet axis, which points directly away from the deeply embedded VLA source VLA 1.

The Herbig-Haro jet is only the optically visible part of the collimated flow from the driving source. Rodríguez *et al.* (1990) studied the source at very high angular

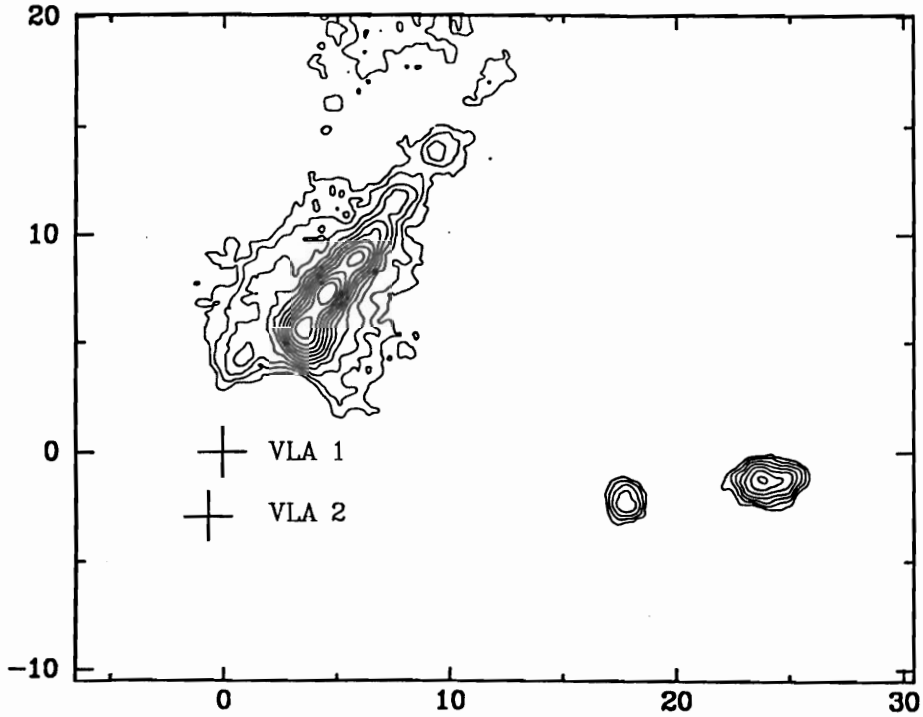

Figure 14. A contour diagram from a [SII] image of the HH 1/2 source region. The HH 1 jet and the two first knots of HH 144 are seen, and the two driving VLA sources are identified. From Reipurth *et al.* (1993a).

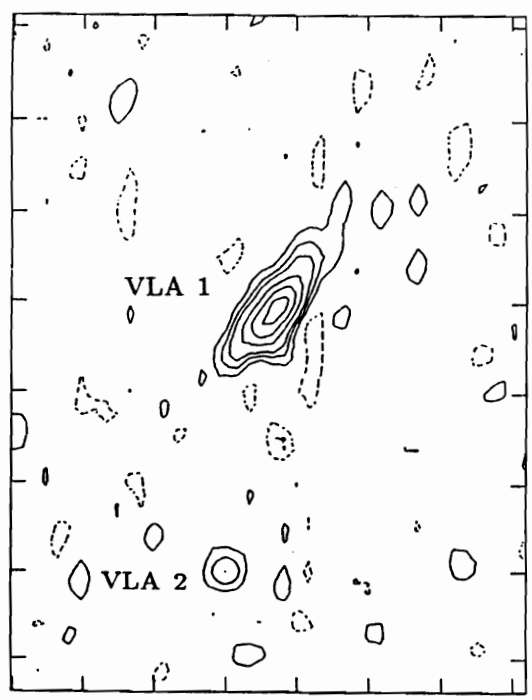

Figure 15. A uniform-weighted VLA map made at 6 cm showing the two embedded sources VLA 1 and VLA 2. VLA 1 shows a tiny well collimated jet pointing towards HH 1. Courtesy L.F.Rodríguez.

resolution with the VLA, and their 6 cm uniform-weighted map of the source region is shown in Fig. 15. They found that VLA 1 is resolved along the jet axis, but unresolved perpendicular to it at a scale of 0.1″, corresponding to about 50 AU. Collimation thus occurs very close to the source. These radio observations are further discussed in Sect. 5.

The deep CCD image in Fig. 13 shows that the two small knots west of the source region are only the brighter parts of a long chain of HH knots called HH 144. Further west a more disorganized group of HH knots, HH 145, is found; its relation to HH 144 is unclear. Proper motion measurements of the two brightest knots in HH 144 show a large transverse motion away from the source region. The alignment of the HH 144 knots suggests that they do not originate from VLA 1, but from a faint source VLA 2, detected in the 6 cm survey of Rodríguez *et al.* (1990), and located 3″ south of VLA 1. A deep infrared K-band image shows two reflection nebulae in the source region, a bright one fanning out from VLA 1 towards HH 1 (e.g. Roth *et al.* 1989), and a faint one stretching from VLA 2 towards HH 144. These multi-wavelength alignments provide strong evidence that HH 1/2 and HH 144 are driven by two independent young stars. Their proximity suggests that they most likely form a physical binary, with a projected separation of 1380 AU.

Millimeter continuum observations at 1300 μm show that VLA 1 and 2 are surrounded by a large extended envelope of cold dust, with a total circumbinary mass of 0.7 to 4.3 $M_\odot$, depending on the choice of mass absorption coefficient. Inside this envelope, the individual stellar components are likely to be surrounded by separate circumstellar disks, because of the relatively large separation of the two components. If the HH flow from each source emerges perpendicular to their surrounding disk, then the disks are not co-planar, but are oriented at a substantial angle to each other. The brightness of the HH 1/2 flow, the brightness of VLA 1 and the fact that the HH 1/2 flow shares the direction of all other flows in this region may suggest that VLA 1 is the main mass in the system, and that it perturbs the smaller mass around VLA 2, setting up a strong precession of the latter's disk.

The dynamical timescale for the HH 144 flow is if the order of 650 yr, assuming a tangential velocity of 350 km s^{-1}. The orbital period has a lower limit of 11500 yr, derived from the projected separation and the assumption that the total binary stellar mass is about 1.5 $M_\odot$, and that about 1 $M_\odot$ of circumstellar material partakes in the orbital motion. Thus, orbital motion has little effect on the appearance of the HH 144 jet.

5. Thermal Radio Jets and Synchrotron Jets

Radio continuum observations at centimeter wavelengths of energy sources of HH jets have shown that some can be detected at these wavelengths. A few are bright enough to be mapped at high resolution, and the maps have revealed tiny well-collimated jets emanating from the embedded sources. The two best examples are the radio jets from L1551 IRS 5 (Bieging & Cohen 1985, Rodríguez *et al.* 1986) and HH 1/2 VLA1 (Rodríguez *et al.* 1990), the latter one is shown in Fig. 15. Both these sources are completely hidden from view by their massive circumstellar environments, and only radio observations offer a way to study them. For the HH 1/2 flow, the minor axis of the radio jet is unresolved, suggesting that collimation is present on scales equal to or smaller than 50 AU. The L1551 radio jet, on the other hand, has been resolved into two compact sources $\sim$ 50 AU apart, which is either a binary (Bieging & Cohen 1985)

or the inner ionized walls of a disk (Rodríguez et al. 1986).

In the case of the HH 1/2 radio jet, which is the best studied of the two, the angular size decreases with increasing frequency and the spectral index is 0.3 (Rodríguez *et al.* 1990), which suggests a confined thermal jet nature (Reynolds 1986). Both of the working surfaces, HH 1 and 2, of the bipolar jet were detected at radio wavelengths with flat spectral indices around 0, consistent with optically thin free-free emission. Observations at several epochs have revealed an oppositely directed tangential motion of the two HH objects away from the central source (Rodríguez *et al.* 1990), in good agreement with the optical proper motions (Herbig & Jones 1981).

Although most embedded outflow sources are not detectable at centimeter wavelengths with present sensitivities, those that can be observed yield very important information because of the high resolution, the ability to penetrate highly obscured regions, and the different physical domain probed by radio observations. Surveys of dark clouds have revealed other bipolar sources, for example Brown (1987) found a double radio source around the embedded infrared source IRS 7 in the Corona Australis dark cloud. This object still awaits high resolution observations, as do a number of objects found in other surveys (e.g. Bieging *et al.* 1984, Curiel *et al.* 1989, Morgan *et al.* 1990).

A particularly interesting object is associated with the embedded far-infrared source Serpens FIRS 1, a 300 $L_\odot$ embedded star. It consists of three aligned sources and is dubbed the Serpens triple source (Rodríguez *et al.* 1980, Snell & Bally 1986). Multi-epoch observations have shown that the two outer components move away from the central radio source with highly supersonic transverse velocities of about 200 km s^{-1} (assuming a distance of 300 pc), suggesting a kinematic age of only about 50 years (Rodríguez *et al.* 1989). Figure 16 shows a new high-resolution VLA map at 3.6 cm of the triple source from Curiel *et al.* (1993), which clearly shows a beautifully collimated jet and two working surfaces. It is particularly noteworthy that, although there obviously is outflowing material on either side of the source, only one side displays an emitting jet. Unlike the situation at optical wavelengths, uneven extinction cannot be invoked for these radio observations.

The multi-frequency study by Rodríguez *et al.* (1989) shows that the central source has a spectral index of $\alpha = 0.1$, suggesting free-free emission, but the two lobes have spectral indices of -0.6 and -0.7, respectively, characteristic of non-thermal synchrotron radiation. This highly unexpected result is not readily explained, since large gravitational potentials are not believed to be present in star forming regions. Contrary to the situation for extragalactic jets, where light travel times to the sources are long compared to the lifetime of the electrons, stellar synchrotron jets could in principle be driven by a central source somehow emitting relativistic electrons (Blome & Kundt 1988). However, a more widely accepted view is that a diffuse shock acceleration mechanism is responsible (Crusius-Wätzel 1990). It is particularly satisfying that both thermal and non-thermal radio jets from young stars can be incorporated in a single scheme, as discussed by Henriksen *et al.* (1991). They give a criterion for when radio jets will be dominated by either thermal or non-thermal emission, which involves the magnetic field strength, the temperature and the density of the outflowing material, and suggest that sources may change with time between thermal and non-thermal behaviour, as these parameters change. The new observations of Curiel et al. (1993) indeed suggest that the spectral indices of the outer components in the Serpens source are changing with time.

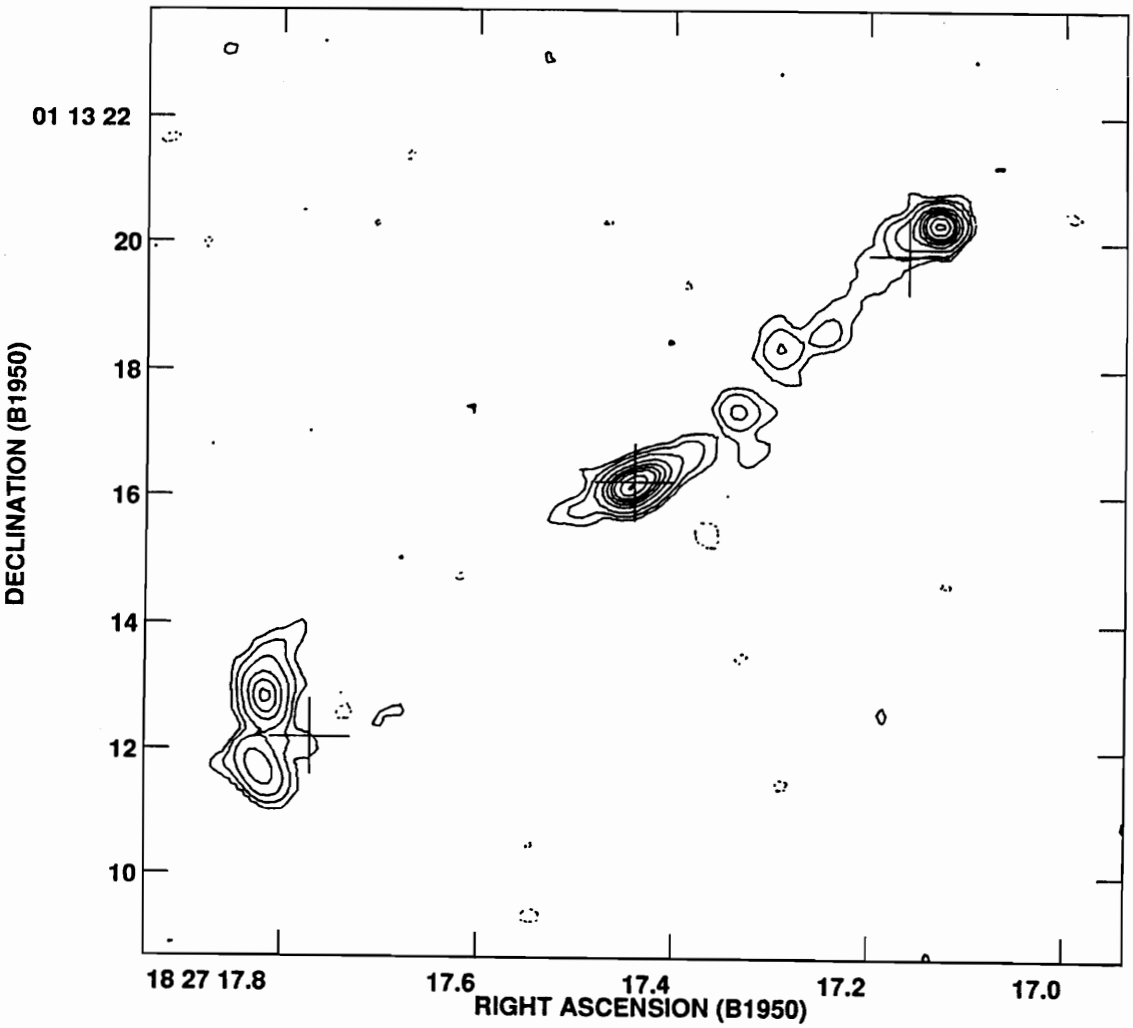

Figure 16. A VLA 3.6cm map of the Serpens triple source with a 1σ noise level of about 13 μJy. The source is a 300 $L_\odot$ deeply embedded young star. The crosses give the positions as observed in 1978, and demonstrate the several hundred km/sec transverse motion of the jet. From Curiel *et al.* (1993).

The synchrotron jet in Serpens is a rare, but not unique object, other non-thermal radio sources are known in star forming regions (e.g. Schwartz *et al.* 1985). The best studied object besides the Serpens triple source is found in Orion and is responsible for a set of optically visible giant shocked arcs, known as the Orion Streamers (Yusef-Zadeh *et al.* 1990), see Fig. 2. The source itself is embedded, but corresponds to a very faint near-infrared source. It has a steep spectral index around -1 and shows a significant degree of linear polarization, about 6%–8% at 6 cm, implying that the magnetic field is highly ordered around the source. A major collimated flow, albeit faint and somewhat diffuse, emanates from the source in a 6 cm map of the region (Yusef-Zadeh *et al.* 1990).

6. Jets from Massive Stars

The jets and flows discussed so far have all emanated from low-luminosity low-mass stars. But a few HH flows from intermediate and higher mass stars have been found (e.g. Axon & Taylor 1984, Reipurth & Graham 1988, Ray *et al.* 1990, Poetzel *et al.* 1992). It is not surprising that HH flows from high luminosity stars are less frequent than from low luminosity stars, because their evolutionary timescales are shorter. Also, the innermost parts of the circumstellar disk of a massive star will be exposed to a very intense UV radiation field, which is likely to rapidly erode the (so far unknown) collimating mechanism. It is noteworthy that HH flows from high luminosity ($> 10^4$ $L_\odot$) stars are principally characterized by their diffuse and poorly collimated morphology. Two particularly interesting regions have been studied in more detail, they are GGD 37 in Cepheus and HH 80/81 in Sagittarius.

The GGD 37 region consists of a large amorphous HH object, GGD 37 itself, which moves north-west, and a smaller HH object moving to the north-east (e.g. Lenzen 1988), away from a small group of radio continuum sources (e.g. Hughes 1985), containing one or more early B stars. Whether or not the two HH objects originate from the same source is not clear.

HH 80/81 are the intrinsically brightest HH objects known, emanating from an embedded high-luminosity IRAS source (Reipurth & Graham 1988). The source is associated with a reflection nebula, GGD 27, and a large bipolar outflow, and is embedded in a dense flattened CS core (Yamashita *et al.* 1989). Compact radio continuum and H_2O maser emission was detected by Rodríguez *et al.* (1980), who suggested a distance of 1.7 kpc. At this distance HH 80/81 lie at a projected distance from the source of 2.3 pc.

Continuum observations of the region were made at 6 cm with the VLA–D array (Rodríguez & Reipurth 1989); both HH 80 and 81 were detected, and the central source was found to be significantly extended in direction towards the HH objects. In a more recent study Martí *et al.* (1993) used the VLA–A array to achieve maps of the region with a resolution of better than 1 arcsec. They found that the central source powers a highly collimated bipolar jet, the central region of which is shown in Fig. 17, and which is unresolved perpendicular to the flow direction. The source is located at the brightest point of the jet. Like jets from low luminosity young stars, the HH 80/81 jet consists of a series of knots. The knots extend beyond the central region shown here, and the south-western lobe points directly towards HH 80 and 81. In the opposite direction, along the well defined flow axis, a radio counterpart to the visible HH objects is found; this object is hidden from view by a large molecular cloud. The total projected extent of this bipolar jet system exceeds 5 pc. The dynamical timescale for the system is not known, because proper motion studies have not yet been carried out, but it is likely to be short, because extremely high radial velocities, up to 700 km s^{-1}, were detected in HH 80/81 (Heathcote and Reipurth 1993).

The case of the HH 80/81 jet system demonstrates that even massive young stars can produce highly collimated bipolar jets, which appear to be rather similar to those from low luminosity young stars, except for being much larger and faster, and probably also considerably more massive.

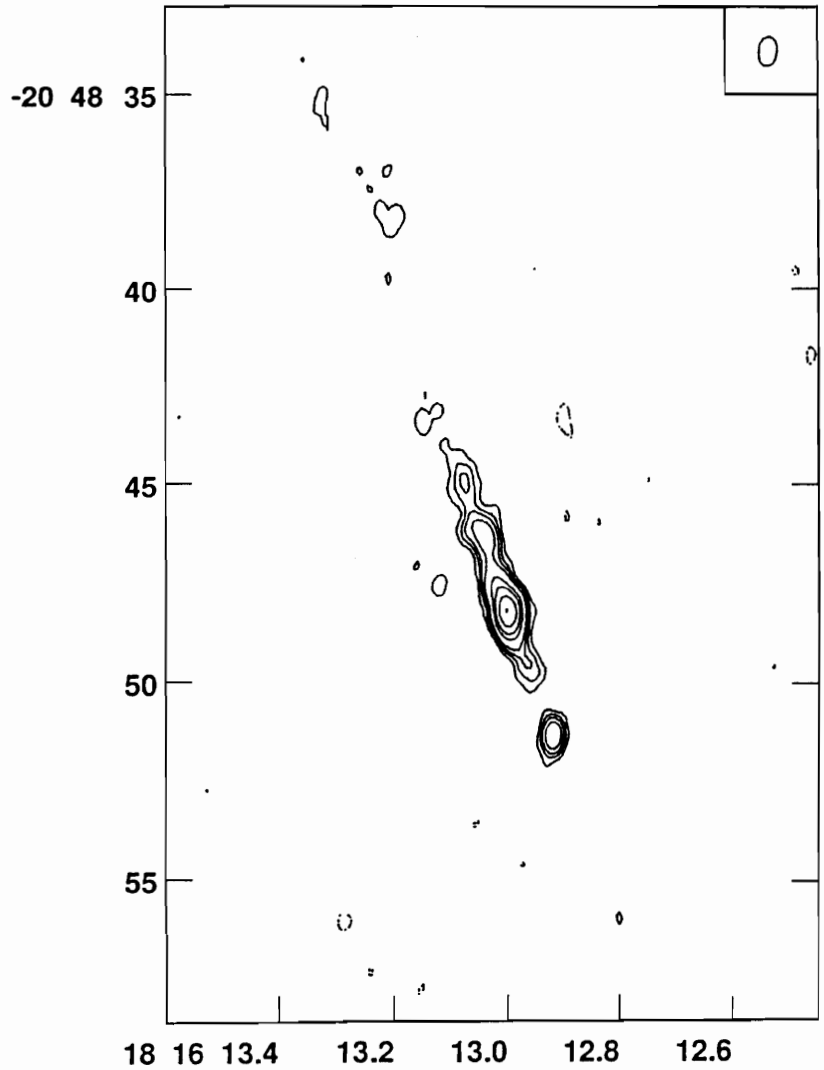

Figure 17. The highly collimated jet in the HH 80/81 complex. The central source is an 18000 $L_\odot$ B star, located in the bright central knot. The map is a 6 cm VLA map. At a distance of 1700 pc, 20 arcsecond correspond to 0.17 pc. From Martí *et al.* (1993).

7. The Energy Sources of Herbig-Haro Jets

Observational clues to the origin and collimation mechanism of Herbig-Haro jets have so far proved elusive, although there is no lack of theoretical ideas, developed in more or less detail. The formation of a jet is almost certainly intimately connected to physical conditions very close to the young star, and we will therefore finish this overview of Herbig-Haro jets with some brief comments on their driving sources.

The majority of HH energy sources are deeply embedded in the molecular clouds in which they formed. Some are visible stars, with larger or smaller amounts of extinction, either because the stars are more evolved and have shed most of their surrounding molecular material, or because they are viewed from a fortuituous direction. A recent study of the IRAS energy distributions of a large compilation of HH energy sources

(Reipurth *et al.* 1993b) has shown that almost all are class I sources, that is, they have spectra rising towards longer wavelengths. Objects with such energy distributions are best interpreted as having circumstellar disks and large infalling envelopes (Adams *et al.* 1987). Statistical studies of young populations in molecular clouds show that the timescale for dispersal of the large envelope is roughly 10^5 yr (e.g. Beichman *et al.* 1986, Parker *et al.* 1991). As a class, HH energy sources are thus among the youngest stars known. 1300μm observations of HH sources reveal that they are still surrounded by large amounts of circumstellar material, from a few tenths to several solar masses (Reipurth *et al.* 1993b).

When visible, HH sources are found to be mostly classical T Tauri stars of the strong emission line type. A few are identified as eruptive variables of the FUor or EXor variety. Such objects are believed to be T Tauri stars which have temporarily undergone eruptions (e.g. Herbig 1977). The decay times of FUors are poorly known, but are suspected to be a hundred to several hundred years, after which they presumably revert to their T Tauri stage. The spectra of FUors have been successfully modelled as resulting from accretion of material through a circumstellar disk at rates of about 10^{-4} $M_{\odot}yr^{-1}$ (e.g. Hartmann & Kenyon 1990). Massive supersonic winds emanate from these objects. EXors may be similar, but scaled-down and shorter-lived accretion events.

It has been suggested that these accretion driven eruptive events are responsible for the HH flows (Dopita 1978, Reipurth 1985b, 1989a, 1991). Dynamic timescales of HH flows are typically a few thousand years. During time intervals of that order the source could have erupted several times, and indeed, as described in section 2.3, the lobes of well collimated jet complexes often contain a series of two or three well defined bow shocks moving out from the source (e.g. Reipurth & Heathcote 1991, 1992, Reipurth *et al.* 1992). Comparing the timescales of the flows and the accretion events, one would expect that the energy sources are seen, most of the time, in their low T Tauri stage rather than in an elevated accretion state, consistent with the available evidence.

Acknowledgements

We are grateful to J. Morse, S. Curiel, and L.F. Rodríguez for permission to show figures 5, 16, and 17 prior to publication, and to A.C. Raga and S. Curiel for comments on the manuscript. B.R. thanks C. Bertout for hospitality at Observatoire de Grenoble, where parts of this review were written.

REFERENCES

Adams, F.C., Lada, C.J., & Shu, F. 1987, *Ap. J.,* **312**, 788.

Axon, D.J. & Taylor, K. 1984, *M.N.R.A.S.,* **207**, 241.

Beichman, C.A., Myers, P.C., Emerson, J.P., Harris, S., Mathieu, R., Benson, P.J., & Jennings, R.E. 1986, *Ap. J.,* **307**, 337.

Bieging, J.H., & Cohen, M. 1985, *Ap. J. (Letters),* **289**, L5.

Bieging, J.H., Cohen, M., & Schwartz, P.R. 1984, *Ap. J.,* **282**, 699.

Blome, H.J., & Kundt, W. 1988, *Ap&SS* **148**, 343.

Blondin, J.M., Fryxell, B.A. & Königl, A. 1990, *Ap. J.,* **360**, 370

Bohigas, J., Torrelles, J. M., Echevarría, J., Cantó, J. Enríquez, R., Firmani, C., Gutiérrez, L., Ruiz, E. & Salas, L. 1985, *Rev. Mexicana Astron. Astrofis.* **11**, 149.

Brown, A. 1987, *Ap. J. (Letters),* **322**, L31.
Bührke, T. Mundt, R. & Ray, T.P. 1988, *Astr. Ap.,* **200**, 99.
Cantó, J., Raga, A.C. & Binette, L. 1989, *Rev. Mexicana Astron. Astrof.,* **17**, 65.
Cohen, M. & Jones, B.F. 1987, *Ap. J.,* **321**, 846.
Crusius–Wätzel, A.R. 1990, *Ap. J. (Letters),* **361**, L49.
Curiel, S., Rodríguez, L.F., Cantó, J., Bohigas, J., Roth, M., & Torrelles, J.M. 1989, *Astro. Lett. and Communications*, **27**, 299.
Curiel,S., Rodríguez, L.F., Moran, J. & Cantó, J. 1993, in preparation
Dopita, M.A., 1978, *Ap. J. Suppl.,* **37**, 117.
Dopita, M.A., Schwartz, R.D., & Evans, I. 1982, *Ap. J. (Letters),* **263**, L73.
Eislöffel, J. & Mundt, R. 1992, *Astr. Ap.,* **263**, 292.
Falle, S.A.E.G., Innes, D.E. & Wilson, M.J. 1987, *M.N.R.A.S.,* **225**, 741.
Graham, J.A., & Elias, J.H. 1983, *Ap. J.,* **272**, 615.
Gredel, R., Reipurth, B. & Heathcote, S.R. 1992, *Astr. Ap.,* **266**, 439
Haro, G. 1952, *Ap. J.,* **115**, 572.
Haro, G. 1953, *Ap. J.,* **117**, 73.
Hartigan, P. 1989 *Ap. J.,* **339**, 987.
Hartigan, P. & Raymond, J. 1993, *in press.*
Hartigan, P., Raymond, J. & Hartmann, L. 1987, *Ap. J.,* **316**, 323.
Hartigan, P., Raymond, J. & Meaburn, J. 1990, *Ap. J.,* **362**, 624.
Hartmann, L. & Raymond, J. 1984 *Ap. J.,* **276**, 560.
Hartmann, L., & Kenyon, S. 1990, *Ap. J.,* **349**, 190.
Heathcote, S.R. & Reipurth, B. 1992, *A. J.,* **104**, 2193
Heathcote, S.R. & Reipurth, B. 1993, in preparation.
Henriksen, R.N., Ptuskin, V.S., & Mirabel, I.F. 1991, *Astr. Ap.,* **248**, 221.
Herbig, G.H. 1950, *Ap. J.,* **111**, 11.
Herbig, G.H. 1951, *Ap. J.,* **113**, 697.
Herbig, G.H. 1974, *Lick Obs. Bull.*, no **658**.
Herbig, G.H. 1977, *Ap. J.,* **217**, 693.
Herbig, G. H. & Jones, B.F. 1981, *A. J.,* **86**, 1232.
Hughes, V.A. 1985, *Ap. J.,* **298**, 830.
Kofman, L. & Raga, A.C. 1992, *Ap. J.,* **390**, 359.
Lenzen, R. 1988, *Astr. Ap.,* **190**, 269.
Martí, J., Rodríguez, L.F., & Reipurth, B. 1993, in preparation.
Meaburn, J., & Dyson, J. 1987, *M.N.R.A.S.,* **225**, 863.
Morgan, J.A., Snell, R.A., & Strom, K.M. 1990, *Ap. J.,* **362**, 274.
Morse, J.A., Hartigan, P., Cecil, G., Raymond, J. & Heathcote, S.R. 1992, *Ap. J.,* **399**, 231.
Morse, J.A., Heathcote, S.R. Cecil, G. Hartigan, P. & Raymond, J. 1993, *in press.*
Mundt, R., Brugel, E. W. & Bührke, T. 1987, *Ap. J.,* **319**, 275.
Norman, M.L. 1993 (these proceedings).
Norman, M.L., Winkler, K.-H. A. & Smarr, L. 1984, in *Physics of Energy Transport in Extragalactic Radio Sources*, eds. A. Bridle & J. Eilek NRAO Greenbank Workshop No 9, p. 150.
Olberg, M., Reipurth, B., & Booth, R. 1992, *Astr. Ap.,* **259**, 252.
Parker, N.D., Padman, R., & Scott, P.F. 1991, *M.N.R.A.S.,* **252**, 442.
Payne, D.G. & Cohn, H. 1985, *Ap. J.,* **291**, 655.

Poetzel, R., Mundt, R. & Ray, T.P. 1992, *Astr. Ap.,* **262**, 229.
Pravdo, S. H., Rodríguez, L. F., Curiel, S., Cantó, J., Torrelles, J. M., Becker, R. H. & Sellgren, K. 1985, *Ap. J. (Letters),* **293**, L35.
Raga, A.C. 1986, *A. J.,* **92**, 637.
Raga, A.C. 1991, *A. J.,* **101**, 1472.
Raga, A.C., Binette, L. & Cantó, J. 1990, *Ap. J.,* **360**, 612.
Raga, A.C. & Böhm, K.-H. 1985, *Ap. J. Suppl.,* **58**, 201.
Raga, A.C. & Böhm, K.-H. 1987, *Ap. J.,* **323**, 193.
Raga, A.C. & Cabrit, S. 1993, in press.
Raga, A.C., Cantó, J., Binette L., & Calvet, N. 1990, *Ap. J.,* **364**, 601.
Raga, A.C. & Kofman, L. 1992, *Ap. J.,* **386**, 222.
Raga, A.C. & Mateo, M. 1988, *A. J.,* **95**, 543.
Raga, A.C., Mateo, M. Böhm, K.-H. & Solf, J. 1988, *A. J.,* **95**, 1783.
Raga, A.C., Mundt, R. & Ray, T.P. 1991, *Astr. Ap.,* **252**, 733
Ray, T.P., Bührke, T. & Mundt, R. 1988, in *NATO-ASI on Formation and Evolution of Low Mass Stars*, eds. A.K. Dupree, & M.T.V.T. Lago, (Dordrecht: Kluwer) p. 281.
Ray, T.P., Poetzel, R., Solf, J. & Mundt, R. 1990, *Ap. J. (Letters),* **357**, L45.
Reipurth, B. 1985a, in *(Sub)-Millimeter Astronomy*, ESO-IRAM-Onsala Workshop, eds. P. Shaver, K.Kjär, p. 459.
Reipurth, B. 1985b, *Astr. Ap.,* **143**, 435.
Reipurth, B. 1989a, *Nature*, **340**, 42.
Reipurth, B. 1989b, in *ESO Workshop on Low Mass Star Formation and Pre-Main Sequence Objects*, ed. Bo Reipurth (Garching: ESO), p. 247.
Reipurth, B. 1990, in *Flare Stars is Star Clusters, Associations and the Solar Neighborhood*, eds. L.V. Mirzoyan *et al.* , IAU Symp No.137, p.229.
Reipurth, B. 1991, in *Physics of Star Formation and Early Stellar Evolution*, eds. C.J. Lada and N. Kylafis, Kluwer, p. 497.
Reipurth, B. 1993, *A General Catalogue of Herbig-Haro Objects*, ESO Scientific Reports, in preparation.
Reipurth, B., Bally, J., Graham, J.A., Lane, A.P. & Zealey, W.J. 1986, *Astr. Ap.,* **164**, 51.
Reipurth, B. & Graham, J.A. 1988, *Astr. Ap.,* **202**, 219.
Reipurth, B. & Heathcote, S.R. 1991, *Astr. Ap.,* **246**, 511.
Reipurth, B. & Heathcote, S.R. 1992, *Astr. Ap.,* **257**, 693.
Reipurth, B., Raga, A.C. & Heathcote, S.R. 1992, *Ap. J.,* **392**, 145.
Reipurth, B., Heathcote, S., Roth, M., Noriega-Crespo, A. & Raga, A.C. 1993a, *Ap. J. (Letters),* in press.
Reipurth, B., Chini, R., Krügel, E., Kreysa, E., & Sievers, A. 1993b, *Astr. Ap.,* in press.
Reynolds, S.P. 1986, *Ap. J.,* **304**, 713.
Roth, M., Tapia, M., Rubio, M. & Rodríguez, L.F. 1989, *Astr. Ap.,* **222**, 211.
Rodríguez, L.F. & Reipurth, B. 1989, *Rev. Mexicana Astron. Astrofis.* **17**, 59.
Rodríguez, L.F., Moran, J.M., Ho, P.T.P. & Gottlieb, E.W. 1980, *Ap. J.,* **235**, 845.
Rodríguez, L.F., Cantó, J., Torrelles, J.M., & Ho, P.T.P. 1986, *Ap. J. (Letters),* **301**, L25.
Rodríguez, L.F., Curiel, S., Moran, J.M., Mirabel, I.F., Roth, M., & Garay, G. 1989, *Ap. J. (Letters),* **346**, L85.

Rodríguez, L.F., Ho, P.T.B., Torrelles, J.M., Curiel, S. & Cantó, J. 1990, *Ap. J.,* **352**, 645.

Schwartz, P.R., Frerking, M.A., & Smith, H.A. 1985, *Ap. J.,* **295**, 89.

Snell, R.L., & Bally, J. 1986, *Ap. J.,* **303**, 683.

Solf, J. 1987, *Astr. Ap.,* **184**, 322.

Solf, J., Böhm, K.H. & Raga, A.C. 1988, *Ap. J.,* **334**, 229.

Stapelfeldt, K.R. Beichman, C.A., Hester, J.J., Scoville, N.Z. & Gautier T.N. 1991, *Ap. J.,* **371**, 226.

Stone, J.M. & Norman, M.L. 1993, *Ap. J.,* in press.

Strom, S. E., Strom, K. M., Grasdalen, G. L., Sellgren, K., Wolff, S., Morgan, J., Stocke, J. & Mundt. R., 1985 *A. J.,* **90**, 2281.

Yamashita, T., Suzuki, H., Kaifu, N., Tamura, M., Mountain, C.M. & Moore, T.J.T. 1989, *Ap. J.,* **347**, 894.

Yusef-Zadeh, F., Cornwell, T.J., Reipurth, B., & Roth, M. 1990, *Ap. J. (Letters),* **348**, L61